Desalination and Water Treatment
www.deswater.com
doi: 10.5004/dwt.2021.26686

212 (2021) 401–414
February

Removal of selected non-steroidal anti-inflammatory drugs from wastewater using reduced graphene oxide magnetite

Awais Zaka[a], Taleb H. Ibrahim[a,*], Mustafa Khamis[b]

[a]*Department of Chemical Engineering, American University of Sharjah, UAE, emails: italeb@aus.edu (T.H. Ibrahim), b00074980@alumni.aus.edu (A. Zaka)*
[b]*Department of Biology, Chemistry and Environmental Sciences, American University of Sharjah, UAE, email: mkhamis@aus.edu*

Received 24 July 2020; Accepted 7 October 2020

ABSTRACT

The efficiency of reduced graphene oxide magnetite (rGOM) to remove selected non-steroidal anti-inflammatory drugs from wastewater at high concentration was evaluated. Diclofenac sodium (DCS) and aspirin (ASP) were chosen as target pharmaceuticals due to their common persistency in wastewater. rGOM was prepared to form graphene oxide (GO) using a one-step procedure where the reduction of GO and attachment of Fe_3O_4 particles to the surface of GO was carried out simultaneously. rGOM showed very good efficiency with percent removal of 98.5% and 90.5% at the optimum conditions for ASP and DCS, respectively. The optimum condition for removal of DCS is adsorbent dosage 14 g L^{-1}, the contact time of 40 min, and a pH of 5.0. While the optimum conditions for ASP are adsorbent dosage 16 g L^{-1}, contact time 40 min, and a pH of 3.0. The adsorption process was evaluated through different adsorption isotherm and kinetic models. Langmuir isotherm model was found to be the best fitting for DCS adsorption with Q_m and K_L values of 12.95 mg g^{-1} and 0.091 L mg^{-1}, respectively. On the other hand, ASP removal was best described by the Freundlich isotherm model with K_F and n values of 5.95 and 2.49, respectively. Both processes showed fast kinetics. Thermodynamic properties were calculated using the Sips isotherm model. The adsorption of both drugs was found to be spontaneous with a negative value of Gibbs free energy and positive enthalpy change indicating that the adsorption process was endothermic. Continuous fixed-bed column adsorption was performed, and the data were fitted using different isotherm models and it was observed that adsorption of DCS follows Yan model while adsorption of ASP is described by Bohart–Adams model. A regeneration study was carried out which showed that the removal efficiency was still significant for both ASP and DCS even after three cycles.

Keywords: Pharmaceuticals; Diclofenac sodium; Aspirin; Reduced graphene oxide magnetite

1. Introduction

Pharmaceuticals have been used from ancient times in different forms for the cure of diseases. The high demand for pharmaceuticals has led to the growth of pharmaceutical manufacturing industries. This pharmaceutical industry comprises more than one million employees and R&D spending of around USD 75 billion [1]. However, gradual growth in the supply and demand of pharmaceuticals have raised a serious concern over the treatment of wastewater generated by these pharmaceutical industries. Pharmaceutical in the water environment enter through various routes and hence induces environmental concerns. This leads to serious pollution of the water body which could not be remediated efficiently with the current technology of wastewater treatment plants [2]. As a result, these

* Corresponding author.

pharmaceuticals find their way into different water bodies causing adverse effects on living organisms even at very low concentrations [3]. Several studies revealed that the presence of these pharmaceuticals in the water body could lead to serious toxic effects on both humans and animals [4–6]. Therefore, innovative methods are needed to remove pharmaceutical compounds from wastewater efficiently.

One of the most widely prescribed classes of pharmaceuticals is non-steroidal anti-inflammatory drugs (NSAIDs). This class is mainly used for the treatment of inflammation, pain reduction, and prevention of blood clots [5,7,8]. Due to their structural stability, NSAIDs are relatively resistive to degradation in the environment and hence these compounds are frequently found in different water bodies [9,10]. Recently, it was reported that diclofenac sodium (DCS) in the marine environment undergo photodegradation yielding different by-products [11]. Long-term exposure to NSAIDs can have adverse effects on different ecological species ranging from fish to birds as well as human beings [12–14]. Hence, the need to remove these compounds before entering the environment should be highly prioritized.

Graphene and graphene-based materials are becoming a prominent topic for research in recent times. The 2-dimensional structure of graphene and its unique properties have opened the gates for its utilization in many fields ranging from electrochemical studies to nanoelectronics [15]. High surface area and good chemical and thermal stability allow the graphene family to be used as an adsorbent in water treatment and removal of pollutants [16]. Graphene oxide (GO) is a compound obtained after the oxidation of graphene through strong oxidizing agents. The surface of GO comprises oxygen-containing functional groups such as hydroxyl, epoxy, carbonyl, and carboxyl thus making it highly hydrophilic and stable [16,17]. Furthermore, the reduction of RO by reducing agents yielded materials called reduced graphene oxide (rGO) that have unique properties [18]. Accordingly, GO and rGO has been successfully used for the removal of different contaminants such as heavy metals and dyes [19–21]. These carbon-based adsorbents have also shown good adsorption capability to remove pharmaceutical compounds from water [22]. However, the difficulty in the separation of adsorbent from the water tends to limit the use of GO and rGO on large scale. Therefore, the need to modify GO particles with other suitable compounds arose. Magnetite nanoparticles (Fe_3O_4) have attracted the attention of researchers due to their suitable properties. These particles have low toxicity and can be easily separated using a magnet. The attachment of magnetite particles to the surface of GO has also shown better adsorption efficiency in some studies [16].

In this study, rGO was found to be more suitable for modification with magnetite nanoparticles than GO. Hence, rGO was selected to be treated with magnetite nanoparticles to obtain reduced graphene oxide magnetite (rGOM) that was successfully characterized. The efficiency of rGOM towards the removal of two selected pharmaceuticals (DCS and ASP) was studied and optimized using the batch process. The adsorption efficiencies are optimized with respect to adsorbent dosage, contact time, pH, initial concentration as well as temperature. The kinetics and thermodynamic of the adsorption process were also studied. Continuous fixed-bed column adsorption was also performed, and the data were fitted using different isotherm models. Regeneration of the adsorbents was also investigated for economical and practical applications. The application of this newly synthesized adsorbent is considered to be novel in its application toward the removal of drugs from pharmaceutical wastewater due to its cost-effectiveness, ease of preparation, and regeneration.

2. Materials and methods

2.1. Materials

Graphene oxide was purchased from Xiamen Tmax Battery Equipment Ltd. (China) and used without any further purification. Analytical grade iron chloride tetrahydrate ($FeCl_3{\cdot}4H_2O$) was obtained from Sigma-Aldrich Inc. (Germany). Double distilled deionized water was used to prepare all solutions. Pure samples of DCS and aspirin (ASP) were obtained from a Local Pharmaceutical Company in UAE and were used as-is. Hydrochloric acid and sodium hydroxide of analytical grades were used for pH adjustments. Analytical grade ammonia (28%) was obtained from Merck Millipore (Germany).

2.2. Instrumentation

Adsorption was carried out in a temperature-controlled multi-stack refrigerated shaking incubator (DAIHAN Scientific, South Korea). Orion 201A+ basic pH meter (Thermo Electron Corporation, USA) was used to measure the pH of the solution. The UV-Vis measurements were carried out using Cary 50 Conc (Varian, Australia), 0.45 μm MCE syringe filters (Chrome Tech, Germany) were used to filter the solution after adsorption experiments and prior to UV-Vis analysis. Samples were dried in an air oven (GALLENKAMP, Weiss Technik, UK). High-resolution images of the adsorbents before and after adsorption of the adsorbates were generated using a scanning electron microscope (TESCAN VEGA.3-LMU, USA). Fourier-transform infrared spectroscopy (FTIR) was recorded using an FTIR spectrometer (Perkin Elmer, USA).

2.3. Methods

2.3.1. Preparation of rGOM (rGO-Fe_3O_4)

rGOM nanocomposite was synthesized using a method described elsewhere [23]. Briefly, 500 mg GO particles were dispersed in 500 mL of distilled water and then sonicated for 3 h at room temperature. Ammonia solution (28%) was then added drop-wise to GO suspension until the pH becomes >11. 10 g of $FeCl_2{\cdot}4H_2O$ was then added very slowly to the suspension. Vigorous stirring was then carried out for 3 h after which the mixture was left overnight at room temperature. The solution was then filtered and washed with distilled water to remove any ammonia before drying at 60°C.

2.3.2. Adsorption experiments

500 mg L^{-1} stock solutions of pharmaceuticals were prepared in distilled water. Batch adsorption experiments

were conducted to quantify the effect of contact time, adsorbent dosage, initial adsorbate concentration, pH, and temperature on the removal efficiency of DCS and ASP by the rGOM. In a typical experiment, a solution of known concentration was prepared in an Erlenmeyer flask. The pH of the solution was adjusted, and a known mass of rGOM was added to the solution before placing it in a shaking incubator at a specified temperature for a pre-determined time. rGOM was then separated from the solution using a syringe filter. The concentration of DCS and ASP was then determined using a UV-vis spectrophotometer from a calibration curve at the analytical wavelength. The removal efficiency was calculated using Eq. (1).

$$\text{Removal } \% = \frac{\left(C_0 - C_e\right)}{C_0} \times 100 \quad (1)$$

where C_0 and C_e are the initial and final concentration of DCS and ASP in mg L^{-1}. Each experiment was performed in triplicates for statistical validation.

2.3.3. Continuous-flow experiments

Continuous-flow experiments were performed in a glass tube with an internal diameter of 1 cm and a length of 50 cm. The adsorbent was placed inside the tube supported by glass wool at the top and bottom to avoid any loss. The flow was adjusted and maintained by the continuous introduction of wastewater from the top of the tube. The volume of water processed was measured after certain time intervals and samples were analyzed using a UV-Vis spectrophotometer. Water containing pharmaceuticals was continuously processed until no change was observed between the initial and final concentrations of pharmaceuticals.

3. Results and discussion

3.1. Characterization of adsorbent

Scanning electron microscopy (SEM) and FTIR techniques were used for the characterization of the different nanomaterials. The FTIR spectra of GO, rGOM, ASP, and DCS rGOM-DCS and rGOM-ASP are shown in Figs. 1 and 2. All the samples show a strong peak at a wavenumber of around 3,400 cm^{-1} indicating the presence of water. Fig. 1d indicates that GO has the following peaks at 2,920; 2,852; 1,720; 1,628; 1,050 and 580 cm^{-1}, indicating the presence of different functional groups on the nanomaterials as described in the introduction [23]. The FTIR spectra of rGOM (Fig. 1c) shows that most of the above peaks are still present except for the one at 1,720 cm^{-1}, with the appearance of new peaks at 800 and 892 cm^{-1}. These changes indicate that rGO was successfully modified to yield rGOM. Figs. 1b and 2b display the FTIR spectra of rGOM loaded with ASP and DCS. Upon comparing these spectra with those of free ASP and DCS reveals that an appearance of the following peaks 750; 1,100; 1,400 and 1,550 cm^{-1} for DCS and the appearance of 600 and 1,550 cm^{-1} peaks for ASP. These observations indicate the successful attachment of these drugs on the rGOM upon adsorption.

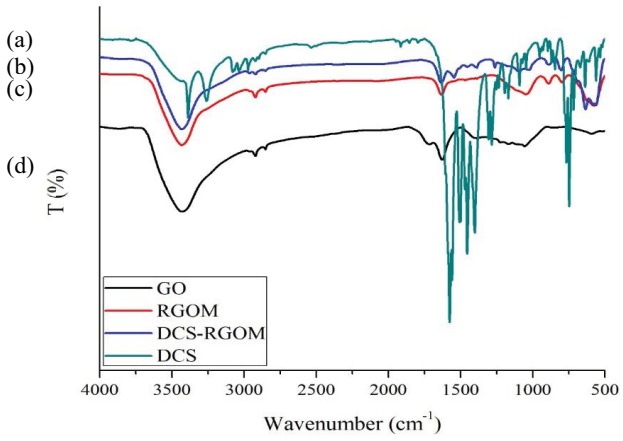

Fig. 1. FTIR spectra of (a) DCS, (b) DCS-rGOM, (c) rGOM, and (d) GO.

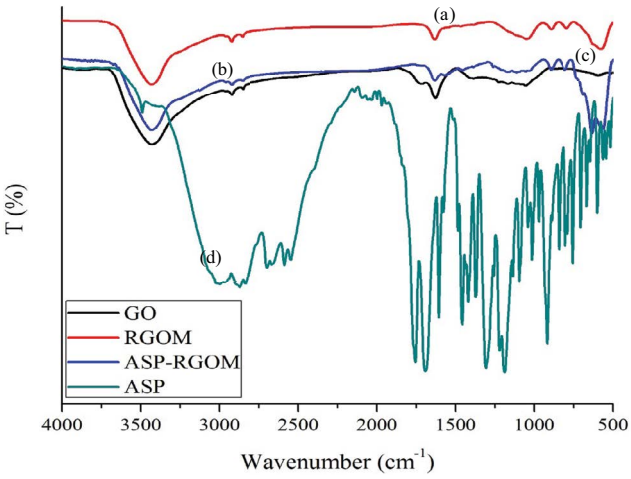

Fig. 2. FTIR spectra of (a) rGOM, (b) ASP-rGOM, (c) GO, and (d) ASP.

Figs. 3a and b show the SEM images of GO and rGOM. It can be clearly observed that the morphology of graphene oxide was changed after the introduction of magnetite particles onto its surface confirming surface modification. Figs. 3c and d show the SEM images of rGOM after it was loaded with DCS and ASP respectively. Clearly, an agglomeration of the rGOM particles can be seen in both images due to both pharmaceuticals, thus confirming the adsorption process.

3.2. Adsorption studies

The first step of this study was to find out the optimum parameters for the removal of both DCS and ASP by rGOM. Dosage of rGOM, contact time between adsorbate and adsorbent, initial concentration of the adsorbate and initial pH of the solution were varied for this purpose. The experiments were carried out at 25°C. The concentration of the pharmaceutical was quantified using UV-vis spectroscopy at λ = 276 nm for DCS and λ = 296 nm for ASP. The effect of each parameter is explained and summarized below.

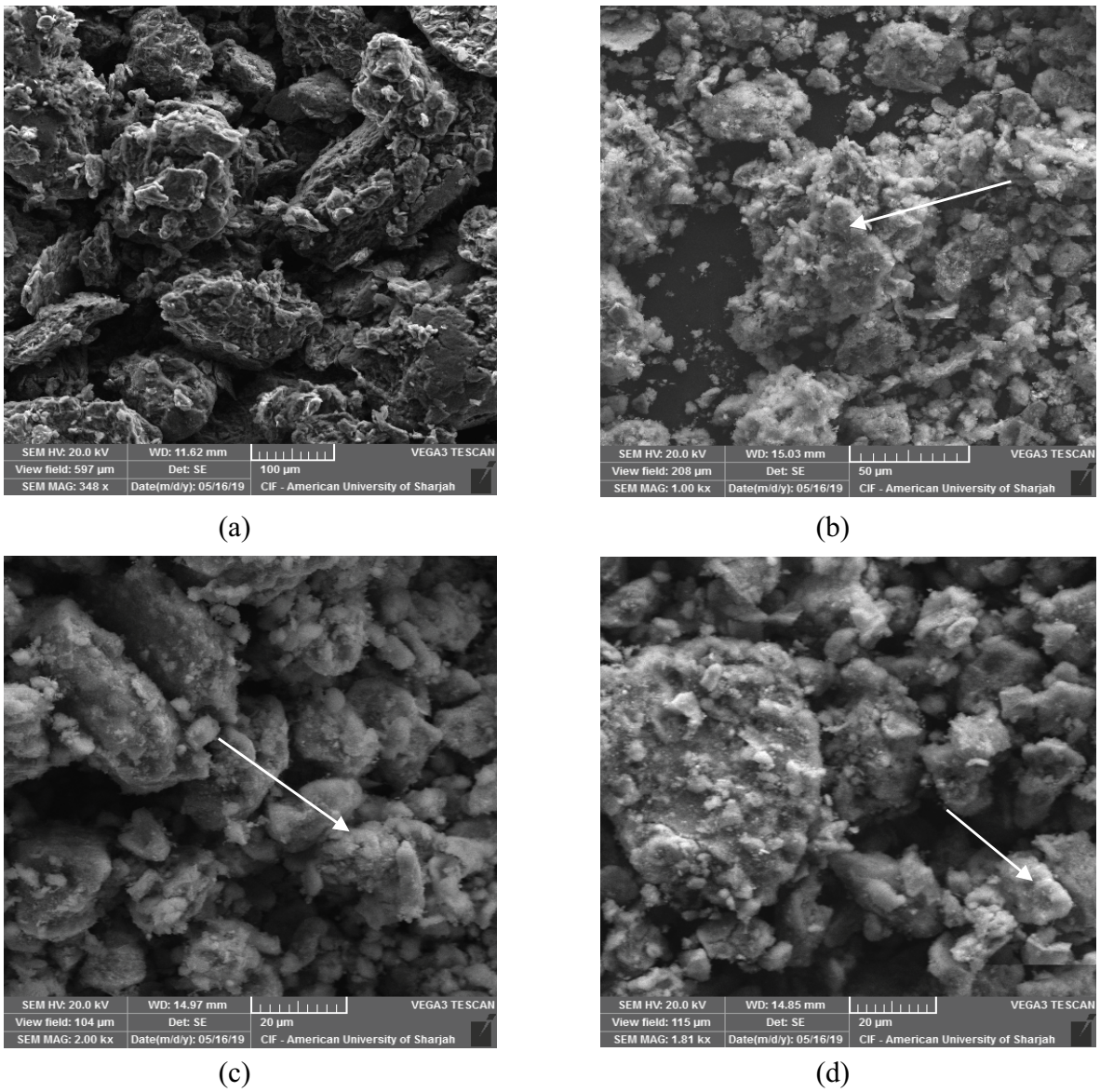

Fig. 3. SEM images of (a) graphene oxide, (b) rGOM, (c) rGOM after adsorption of DCS, and (d) rGOM after adsorption of ASP.

3.2.1. Effect of adsorbent dosage

Dosage of the adsorbent is a very important parameter for practical application of the process as the economics of the system are heavily dependent on it. In this experiment, the dosage of rGOM was varied between 8.0 to 20.0 g L^{-1}, and the percent removal of ASP and DCS was calculated. Fig. 4 displays the effect of the dosage on the percent removal of each drug. The inspection of this figure reveals that increasing the dosage of rGOM is accompanied by an increase in the removal efficiency of both DCS and ASP. This observation could be explained based on the availability of adsorption sites. As the dosage increase, the available sites increase. However, after a certain value, the removal efficiency became constant. This observation could be attributed to either the non-availability of driving forces for adsorption under specified conditions [24] or to the saturation of available active sites. Based on the experimental results, a dosage of 14 and 16 g L^{-1} was selected as the optimum dosage for DCS and ASP, respectively.

3.2.2. Effect of contact time

The effect of contact time on the percent removal of both drugs is shown in Fig. 5. Both DCS and ASP showed fast kinetics with more than 80% removal within the first 10 min. The percent removal then remains almost constant. It is known that the physisorption process does not require any activation, hence results in fast kinetics. On the other hand, chemisorption could be either fast or slow depending on the activation energy of the process [25]. Based on these data alone, the nature of the adsorption process could be associated with neither physisorption nor chemisorption. Further experiments are needed for such identification. A contact time of 40 min was chosen as the optimum value of the removal for both DCS and ASP.

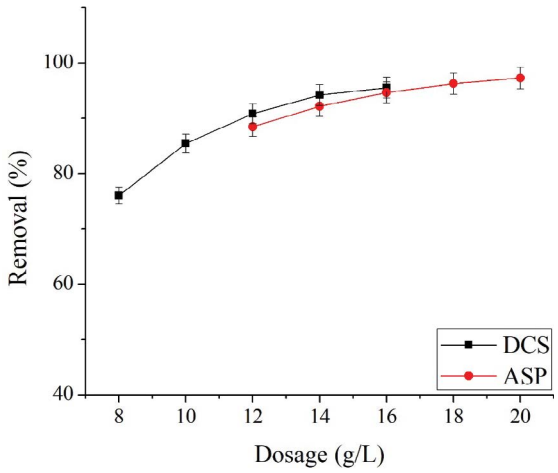

Fig. 4. Effect of dosage on the removal of DCS and ASP using rGOM. Shaker speed: 175 rpm; contact time: 120 min; initial concentrations of DCS and ASP: 100 mg L^{-1}; pH: 5 ± 0.1 for DCS and 3 ± 0.1 for ASP; temperature: 25°C.

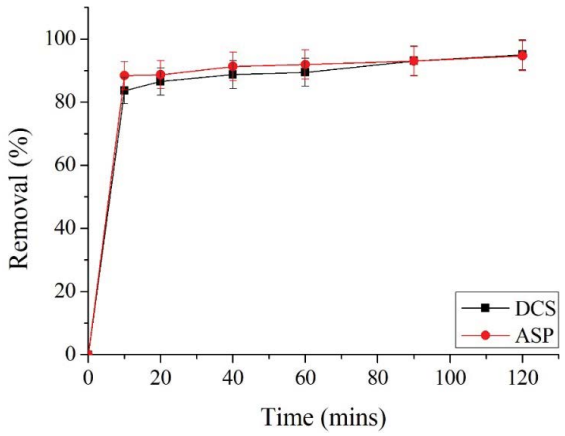

Fig. 5. Effect of time on the removal of DCS and ASP using rGOM. Shaker speed: 175 rpm; dosage: 14 g L^{-1} for DCS and 16 g L^{-1} for ASP; initial concentrations of DCS and ASP: 100 mg L^{-1}; pH: 5 ± 0.1 for DCS and 3 ± 0.1 for ASP; temperature: 25°C.

3.2.3. Effect of pH

pH plays a significant role in the adsorption process helping in understanding the mechanism of the process along with the species taking part in the adsorption. It can be observed from Fig. 6 that both DCS and ASP show high removal at low pH values while the removal decreases slightly as the pH become basic. Maximum removal for DCS was observed at a pH of 5 while ASP showed maximum removal at pH 3. These values were taken as the optimum pH for the removal of both drugs.

To understand the behavior of removal efficiency as a function of pH, it is better to investigate the nature of charges on the surface of the adsorbent as well as the nature of the stable form of the adsorbate at that pH. The dissociation of DCS and ASP along with pKa values are shown in Fig. 7. Tayyebi and Outokesh [26] showed that the surface of rGOM carries a positive charge at pH below 1.9 and remains negatively charged above this value. Hence, it is expected that the removal efficiency of both drugs to be high when they carry either a positive charge or neutral. Inspection of Fig. 6, reveals that the percent removal of DCS is high at low pH and decreases of increasing pH. Fig. 7 indicates that the pK_a value of DCS is 4.35, hence it is present as neutral species at low pH and negatively charged ion at high pH. These properties indicate that at low pH van der Waals forces play a major role in the adsorption process; however, electrostatic repulsion is taking over at high pH. Hence, this prediction is an acceptable explanation of the observed dependence of the percent removal of DCS on pH. On the other hand, aspirin has a point of pK_a of 3.5, indicating that the predominant species at pH < 3.5 is neutral in nature whereas it becomes negatively charged ion at higher pH. Hence, it is expected that the percent removal to be controlled by van der Waals forces at low pH and electrostatic repletion at high pH. These predictions can successfully explain the observed results in Fig. 6.

3.2.4. Effect of initial adsorbate concentration

The effect of initial concentrations of ASP and DCS on the percent removal of both drugs by rGOM is shown in Fig. 8. Initial concentrations of both pharmaceuticals were varied from 100 to 300 mg L^{-1}. The results show that a decrease in the percent removal of both drugs were observed as initial concentration increases. This observation could be explained on basis of the saturation of rGOM sites at a high pharmaceutical concentration as predicted by the Langmuir adsorption model (Eq. (3)).

3.2.5. Effect of temperature

Fig. 9 shows the effect of temperature on the percent removal of both drugs by rGOM at the optimum conditions. Fig. 9 reveals that the percent removal for both drugs is slightly decreasing with increasing temperature. However, the large standard deviation in the data prevents a solid conclusion about the thermodynamic nature of the process. Other methods should be used to evaluate the thermodynamic parameters as described in the pertaining section below.

3.3. Adsorption isotherms

Langmuir, Freundlich, and Temkin isotherm models were utilized to fit the adsorption data in order to have a better understanding of the adsorption mechanism. The experiments were performed at optimum conditions while varying the concentrations of DCS and ASP. The drug adsorption capacity at equilibrium (Q_e) was calculated using Eq. (2):

$$Q_e = \frac{\left(C_0 - C_e\right)V}{m} \tag{2}$$

where Q_e (mg g^{-1}) is the amount of DCS and ASP adsorbed per gram of rGOM, C_0 and C_e are the initial and equilibrium concentrations (mg L^{-1}) of DCS and ASP, respectively.

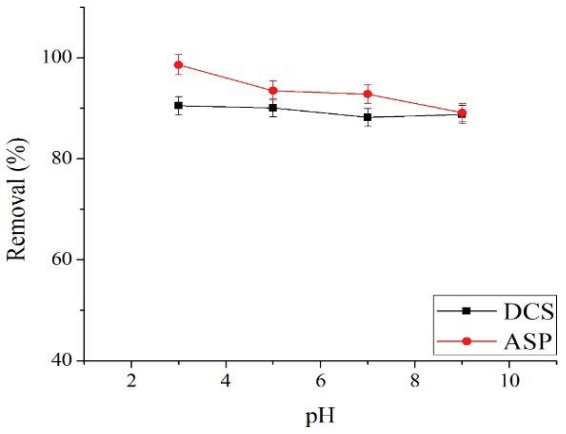

Fig. 6. Effect of pH on the removal of DCS and ASP using rGOM. Shaker speed: 175 rpm; dosage: 14 g L^{-1} for DCS and 16 g L^{-1} for ASP; initial concentrations of DCS and ASP: 100 mg L^{-1}; contact time: 40 min; temperature: 25°C.

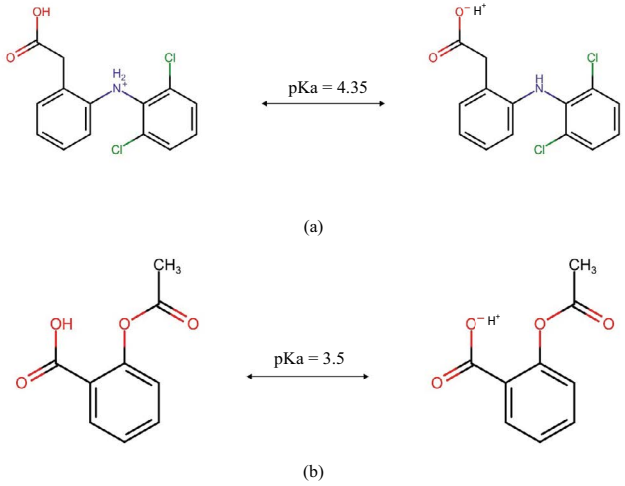

Fig. 7. Dissociation of pharmaceuticals (a) diclofenac sodium (pKa = 4.15) and (b) aspirin (pKa = 3.5).

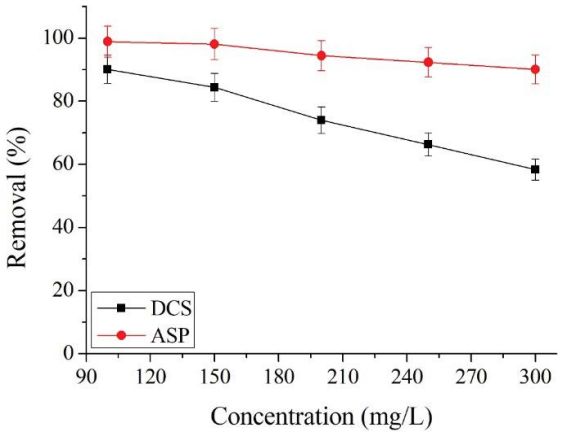

Fig. 8. Effect of initial concentration on the removal of DCS and ASP using rGOM. Shaker speed: 175 rpm; dosage: 14 g L^{-1} for DCS and 16 g L^{-1} for ASP; pH: 5 ± 0.1 for DCS and 3 ± 0.1 for ASP; contact time: 40 min; temperature: 25°C.

V (L) is the volume of the solution and m (g) is the mass of rGOM used in an experiment. Fig. 10 display the dependence of Q_e on the equilibrium concentration at 25.0°C. The observed adsorption curves for both DCS and ASP represent type 1 adsorption isotherm in which monolayer formation is obtained [27]. To model the adsorption process, Langmuir, Freundlich, and Temkin models were employed. The linear forms of these models are given in Eqs. (3)–(5), respectively [28].

$$\frac{C_e}{Q_e} = \frac{C_e}{Q_m} + \frac{1}{Q_m K_L} \tag{3}$$

$$\log Q_e = \log K_F + \frac{1}{n}\log C_e \tag{4}$$

$$Q_e = B\ln K_T + B\ln C_e \tag{5}$$

where Q_m (mg g^{-1}) is the maximum adsorption capacity, K_L (L mg^{-1}) is the Langmuir isotherm constant, K_F ($mg^{(1-1/n)}$ $L^{1/n}$ g^{-1}) and n are the Freundlich isotherm constants and B (J mol^{-1}) and K_T (L mg^{-1}) are Temkin isotherm constants. Fig. 11 display the plot of each isotherm together with their regression coefficients (R^2). Inspection of this figure reveals that the Langmuir isotherm model is best describes the adsorption isotherm for DCS, whereas the Freundlich isotherm model was found to be best to describe the adsorption isotherm for ASP. Table 1 summarizes the isotherm constants for the removal of DCS using the Langmuir model and the removal of ASP using the Freundlich model.

A comparison of maximum adsorption capacity (Q_m) of different adsorbents used for the removal of DCS and ASP is shown in Table 2. It can be observed from the table that the obtained values of Q_e in this work is low as compared to other adsorbents. Inspection of this table reveals that it is tempting to render the single-layered graphene oxide and 3D graphene structure to be the most

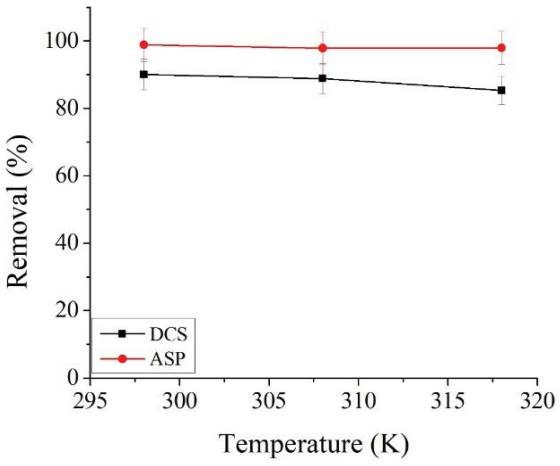

Fig. 9. Effect of temperature on the removal of DCS and ASP using rGOM. Shaker speed: 175 rpm; dosage: 14 g L^{-1} for DCS and 16 g L^{-1} for ASP; pH: 5 ± 0.1 for DCS and 3 ± 0.1 for ASP; contact time: 40 min; initial concentrations of DCS and ASP: 100 mg L^{-1}.

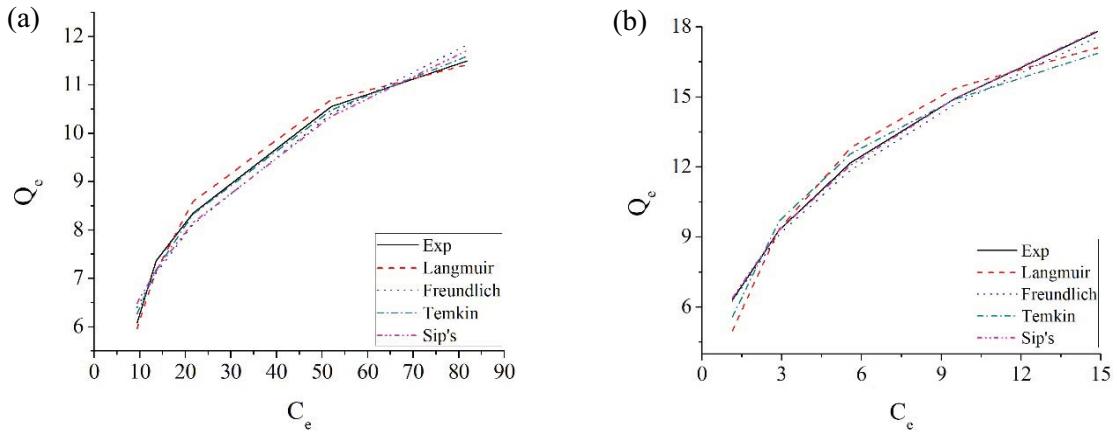

Fig. 10. Adsorption isotherm models for DCS and ASP removal. (a) Langmuir isotherm model, (b) Freundlich isotherm model, and (c) Temkin isotherm model. Experimental conditions: shaker speed: 175 rpm; contact time = 40 min; pH = 5 ± 0.1 for DCS and 3 ± 0.1 for ASP; rGOM dosage = 14 g L^{-1} for DCS and 16 g L^{-1} for ASP; temperature = 25°C.

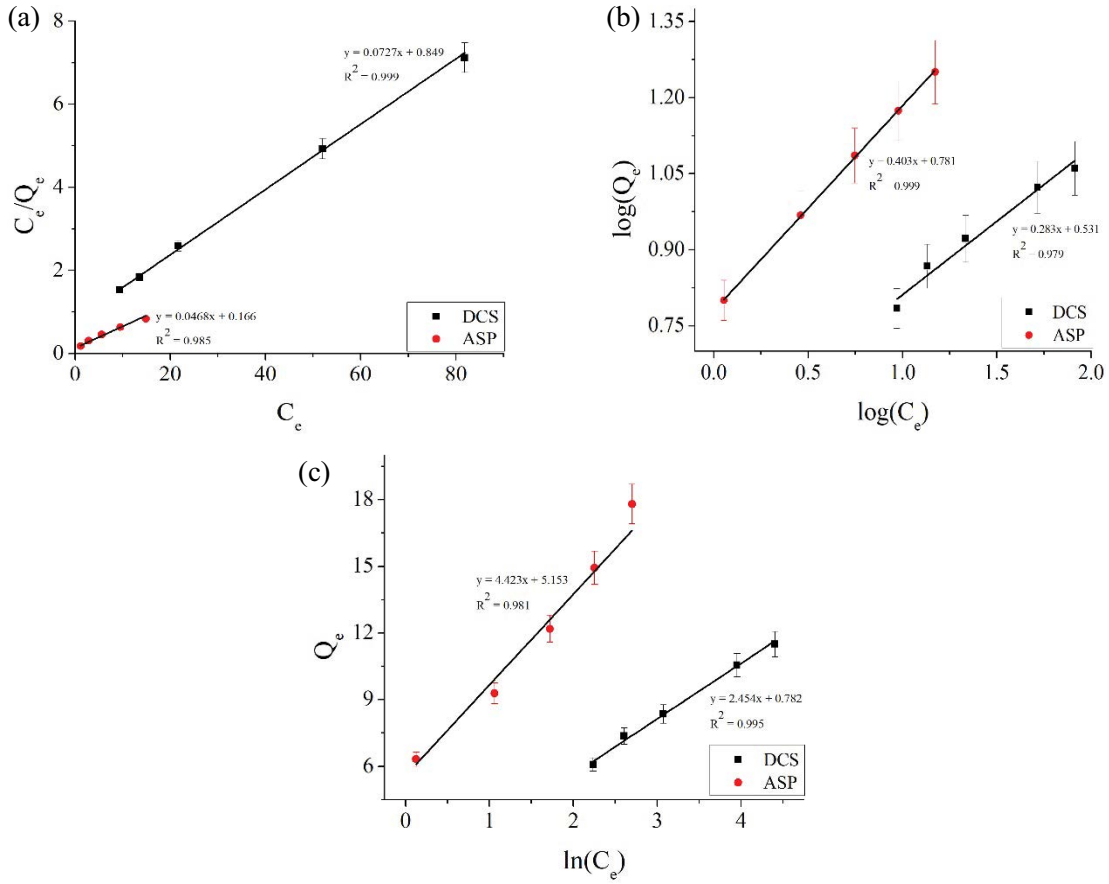

Fig. 11. Comparison of different isotherm models used to fit the data (a) DCS and (b) ASP.

practical adsorbents for the removal of these drugs from the environment. However, the economical preparation of these adsorbents is highly costly which hinders their application. The low values of Q_m for both drugs appear to hinder their practical applications, however, the high density of rGOM and its easy recovery by simple magnets in batch sequential contactors overcome this disadvantage. Hence, our study contributes to the novelty of the removal of these drugs in a natural environment with minimum operational cost.

Table 1
Adsorption isotherms parameters for the removal of DCS and ASP by rGOM at 25°C

Model	Adsorption parameters		
		DCS	ASP
Langmuir	K_L (L mg^{-1})	0.091	0.267
	Q_m (mg g^{-1})	13.76	21.41
	R^2	0.999	0.989
Freundlich	K_F (mg$^{(1-1/n)}$ L$^{1/n}$ g^{-1})	3.39	5.95
	n	3.53	2.49
	R^2	0.978	0.999

3.4. Adsorption thermodynamics

A clear picture of adsorption phenomena cannot be obtained without studying the thermodynamics of the process. The value of different thermodynamic properties such as Gibbs free energy, enthalpy, and entropy is vital to understand the feasibility and thermal aspects of adsorption [38]. In order to calculate the above-mentioned properties, Sips equation [44] was used which is given in Eq. (6).

$$Q_e = Q_e^{\text{th}} \frac{K_{\text{eq}} C_e^{n_s}}{1 + K_{\text{eq}} C_e^{n_s}} \tag{6}$$

where Q_e^{th} (mg g^{-1}) is the maximum theoretical capacity and n_s is the Sips constant. Eq. (6) was used to estimate the equilibrium constant, K_{eq} as a function of temperature. Once the value of Q_e^{th}, n_s, and K_{eq} was determined after regression analysis, the van't Hoff plot was obtained, and it is shown in Fig. 12. The values of the parameters calculated are shown in Table 3. The change in Gibbs free energy was calculated using Eq. (7) given by Yu et al. [45].

$$\Delta G = -RT \ln K_{\text{eq}} \tag{7}$$

where R (J mol^{-1} K^{-1}) is the general gas constant, and T (K) is the temperature. The values of other thermodynamic parameters were calculated using the van't Hoff Eq. (8).

$$\ln K_{\text{eq}} = -\frac{\Delta H}{RT} + \frac{\Delta S}{R} \tag{8}$$

Although the van't Hoff plot for DCS gave a linear relation, the graph for ASP was curved and therefore the above equation cannot be used. A polynomial fit was suggested for such processes where enthalpy does not remain constant with respect to temperature [46]. The equation used for the case of ASP adsorption is given as:

$$\ln K_{\text{eq}} = a + \frac{b}{T} + \frac{c}{T^2} \tag{9}$$

where

$$\Delta H = -R\left(b + \frac{2c}{T}\right) \tag{10}$$

Table 2
Comparison of adsorbent capacities of different adsorbents

S. No.	Adsorbent	Maximum adsorption capacity (mg g^{-1})	References
	Adsorption of DCS		
1	Carbon nanotubes (CNT)	27	[29]
2	Commercial activated carbon	76	[30]
3	Activated carbon (AC) derived from cocoa shell	63	[31]
4	Single layered graphene oxide (GO)	750.0	[32]
5	Reduced graphene oxide (rGO)	59.67	[33]
6	3D graphene aerogel	596.71	[34]
7	CTAB-ZIF-67	54.31	[35]
8	CNT/HNO_3	24	[36]
9	AC derived from olive stones	11	[37]
10	rGO-magnetite	12.95	This study
	Adsorption of ASP		
1	Graphene nanoplatelets	12.98	[38]
2	Activated carbon (AC) derived from rice hull	178.98	[39]
3	Activated carbon (AC) derived from tea leaves	178.5	[40]
4	N-CNT/β-cyclodextrin NC	72	[41]
5	Fe/N-CNT/β-cyclodextrin NC	71.9	[41]
6	Molecularly imprinted polymer	0.03	[42]
7	Tyre waste	40.40	[43]
8	rGO-magnetite	21.41	This study

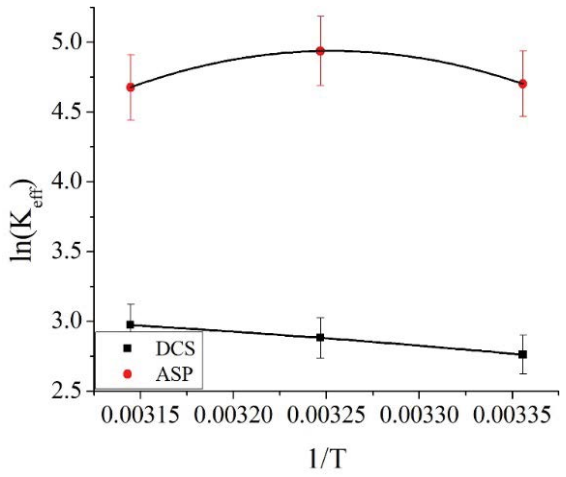

Fig. 12. Van't Hoff plot. Experimental conditions: shaker speed: 175 rpm; contact time = 40 min; pH = 5 ± 0.1 for DCS and 3 ± 0.1 for ASP; rGOM dosage = 14 g L^{-1} for DCS and 16 g L^{-1} for ASP; initial concentrations of DCS and ASP: 100 mg L^{-1}.

Table 3
Calculated Sips parameters at different temperatures

Temperature (K)	DCS		ASP	
	K_{eq}	n_s	K_{eq}	n_s
298.1	15.84	3.670	114.45	2.474
308.1	17.85	3.402	384.64	1.879
318.1	19.56	3.268	80.65	2.595

and

$$\Delta S = R\left(a - \frac{c}{T^2}\right) \tag{11}$$

The values of thermodynamic properties obtained are given in Table 4. The value of Gibbs free energy shows that the process of adsorption for both pharmaceuticals is physical in nature (between –20 to 0 kJ mol^{-1}) while the negative sign is an indication of the spontaneous nature of the process. Moreover, the positive value of enthalpy (ΔH) for aspirin implies that the adsorption is endothermic in nature. The positive sign of entropy change for DCS adsorption shows an increase in the randomness of the system [47]. Negative values of entropy were observed for ASP which was strongly affected by temperature.

3.5. Continuous fixed-bed column adsorption

Apart from batch experiments, a fixed bed adsorption study is useful for the industrial applicability of water treatment through adsorption. In this method, the system is most likely to be far from equilibrium and hence the removal efficiency is affected by additional parameters such as column depth, flow rate, and column diameter [48]. In particular, the interpretation of the removal efficiency in a packed bed column depends on several factors such as adsorption kinetics, resistance to film, diffusion mechanism, and dispersions in liquid flow. Several models for the removal of pollutants in a fixed bed column are reported in the literature such as the Thomas model, Bohart–Adams model, Clark model, and Yan et al. model [24]. These models are applied in this study for the interpretation of the experimental breakthrough curves. The linearized form of each model is given in Eqs. (14)–(17), respectively.

$$\ln\left(\frac{C_0}{C_t} - 1\right) = \frac{K_{TH} q_0 m}{Q} - K_{TH} C_0 t \tag{12}$$

$$\ln\left(\frac{C_t}{C_0}\right) = K_{AB} C_0 t - K_{AB} N_0 \left(\frac{Z}{U_0}\right) \tag{13}$$

$$\ln\left(\left(\frac{C_0}{C_t}\right)^{n-1} - 1\right) = \ln A - rt \tag{14}$$

$$\ln\left(\frac{C_0}{C_0 - C_e}\right) = a \ln V - a \ln b \tag{15}$$

where C_0, C_t, t and n are the initial concentration of the pharmaceutical (mg L^{-1}), the concentration of pharmaceutical at any time (mg L^{-1}), time (min) and Freundlich parameter, respectively. K_{TH} and K_{AB} are the rate constants for Thomas and Bohart–Adams model, respectively. A and r are parameters for the Clark model. V is the volume (mL) whereas a and b are the parameters for Yan model. Z is the bed depth (cm), N_0 is the saturation concentration (mg L^{-1}), U_0 is the superficial velocity (cm min^{-1}), Q is the flow rate (mL min^{-1}) and q_0 is the adsorption capacity (mg g^{-1}).

3.5.1. Effect of flow rate

The effect of flow rate on the breakthrough point for the removal of the DCS and ASP with an initial concentration of 100 mg L^{-1} and bed depth of 1.8 cm is shown

Table 4
Thermodynamic properties

	DCS			ASP		
T (K)	298.1	308.1	318.1	298.1	308.1	318.1
ΔG (kJ mol^{-1})	–6.848	–7.384	–7.865	–11.75	–14.75	–10.88
ΔH (kJ mol^{-1})	8.315			93.44	129.6	163.5
ΔS (J mol^{-1} K^{-1})	50.905			–53.51	–172.9	–281.2

in Figs. 13a and b. Inspection of Fig. 13 reveals that DCS (Fig. 13a) and ASP (Fig. 13b) shows completely different behavior in terms of breakthrough points. The removal of ASP (Fig. 13b) remains high in the initial phase of the process reaching the breakthrough points at 220 and 170 mL using a flow rate of 0.45 and 0.65 mL min^{-1}, respectively. On the other hand, the breakthrough point for DCS is reached much faster at 20 mL and seems to be independent of the flow rates used. The apparent decrease in the breakthrough point of ASP as a function of the flow rate can be explained on the basis that increase in flow rate results in decreasing contact time and hence a decrease in the adsorption capacity and service time of the column.

3.5.2. Effect of bed depth

The effect of the bed depth of adsorbent in a fixed-bed column is shown in Fig. 14. It is evident from the figure that the increase in the bed depth from 1.8 to 3.6 cm results in increasing the breakthrough point from 200 to 400 mL in the case of ASP (Fig. 14b). On the other hand, and since the Q_m for DCS is low, no apparent effect of bed depth on the breakthrough point is observed for DCS (Fig. 14a). The increase in breakthrough points in the case of ASP could be attributed to the availability of more active sites as a result of larger bed depth [48].

3.5.3. Fixed-bed adsorption models

Different models used to fit the adsorption data for fixed-bed adsorption of DCS and ASP are shown in Figs. 15 and 16, respectively. The highest value of R^2 for the adsorption of DCS was observed for Yan model. Yan model is based on the assumption that the adsorption process follows the Langmuir isotherm model and suggests that the rate-limiting step is not defined by internal and external diffusion [49] and the results obtained for DCS are similar to previously reported studies [50]. On the other hand, Bohart–Adams model was found to fit the data obtained from ASP adsorption. It assumes that the rate of uptake of the adsorbate is proportional to the concentration of adsorbate in the bulk liquid and the residual adsorptive capacity of the adsorbent. Bohart–Adams model takes several factors into account such as bed depth (cm) and superficial velocity (cm min^{-1}) of the fluid and the effect of each parameter can be approximately estimated [51]. The calculated regression coefficients (R^2) along with different model parameters are summarized in Table 5.

Table 5
Continuous fixed-bed adsorption model parameters for the removal of DCS and ASP using rGOM

Adsorption models	Parameters		DCS	ASP
Thomas	K_{TH}	L mg^{-1} min^{-1}	0.206	0.182
	q_0	mg g^{-1}	5.249	23.59
	R^2	–	0.859	0.8257
Bohart–Adams	K_{AB}	L mg^{-1} min^{-1}	0.049	0.128
	N_0	mg L^{-1}	10,227.2	16,830.5
	R^2	–	0.389	0.922
Clark	A	–	54.05	13236
	r	min^{-1}	0.025	0.024
	R^2	–	0.742	0.867
Yan	a	–	3.1414	2.112
	b	mL	48.522	336.771
	R^2	–	0.9583	0.5256

3.6. Regeneration study

Reusability study is one of the most important aspects of adsorption. A good adsorbent must retain its capacity to adsorb the pollutants after several cycles and should be easily regenerated. rGOM was reused for three cycles in batch adsorption mode. Regeneration was performed after each cycle using a 0.01 M NaOH solution. In a typical experiment, the optimum amount of rGOM was mixed with pharmaceutical solutions at the optimum pH. After the completion of adsorption, rGOM was separated from the solution, mixed with 100 mL of 0.01 M NaOH solution, and then sonicated for 2 h. The adsorbent is then filtered, washed with warm water (at 60°C), and then dried at 120°C. The results from the regeneration and reusability study are

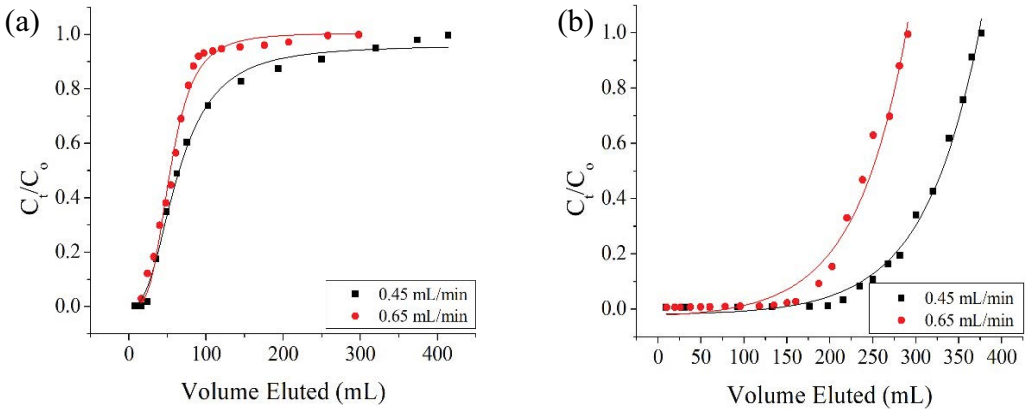

Fig. 13. Effect of flow rate of solution on the removal of (a) DCS and (b) ASP by using rGOM. Bed depth = 1.8 cm; pH = 5 ± 0.1; initial concentration = 100 mg L^{-1}; temperature = 25°C.

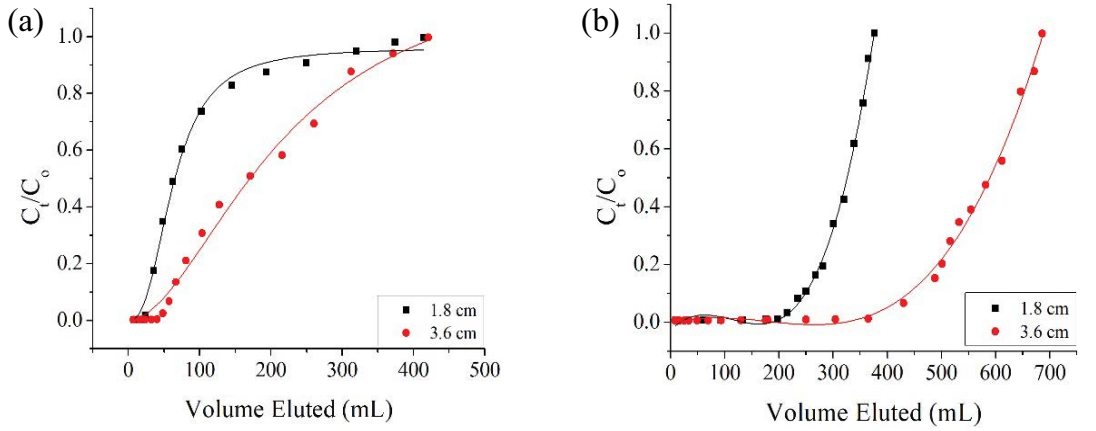

Fig. 14. Effect of bed depth of rGOM on the removal of (a) DCS and (b) ASP by using rGOM. Flow rate = 0.45 mL min^{-1}; pH = 5 ± 0.1; initial concentration = 100 mg L^{-1}; temperature = 25°C.

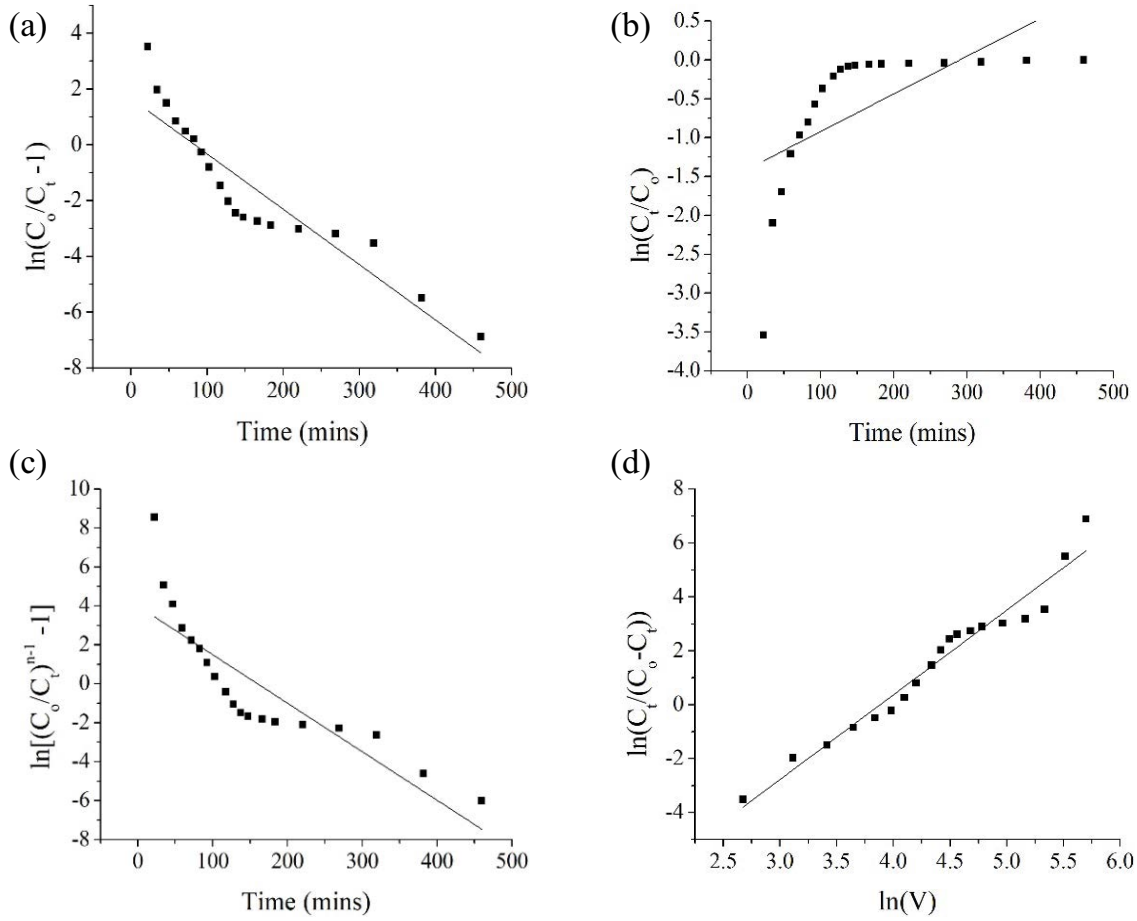

Fig. 15. (a) Thomas, (b) Bohart–Adams, (c) Clark, and (d) Yan model for fixed-bed adsorption of DCS using rGOM. Flow rate = 0.65 mL min^{-1}; bed depth = 1.8 cm; pH = 5.0 ± 0.1; initial concentration = 100 mg L^{-1}; temperature = 25°C.

shown in Fig. 17. It can be observed that the removal efficiency remains above 60% for DCS and above 75% for ASP even after three cycles of regeneration and reuse. Hence rGOM can be successfully applied for the removal of anti-inflammatory drugs from industrial wastewater.

4. Conclusions

rGOM was used as an adsorbent for the removal of two very common anti-inflammatory drugs, namely DCS and aspirin. The removal efficiency was found to be

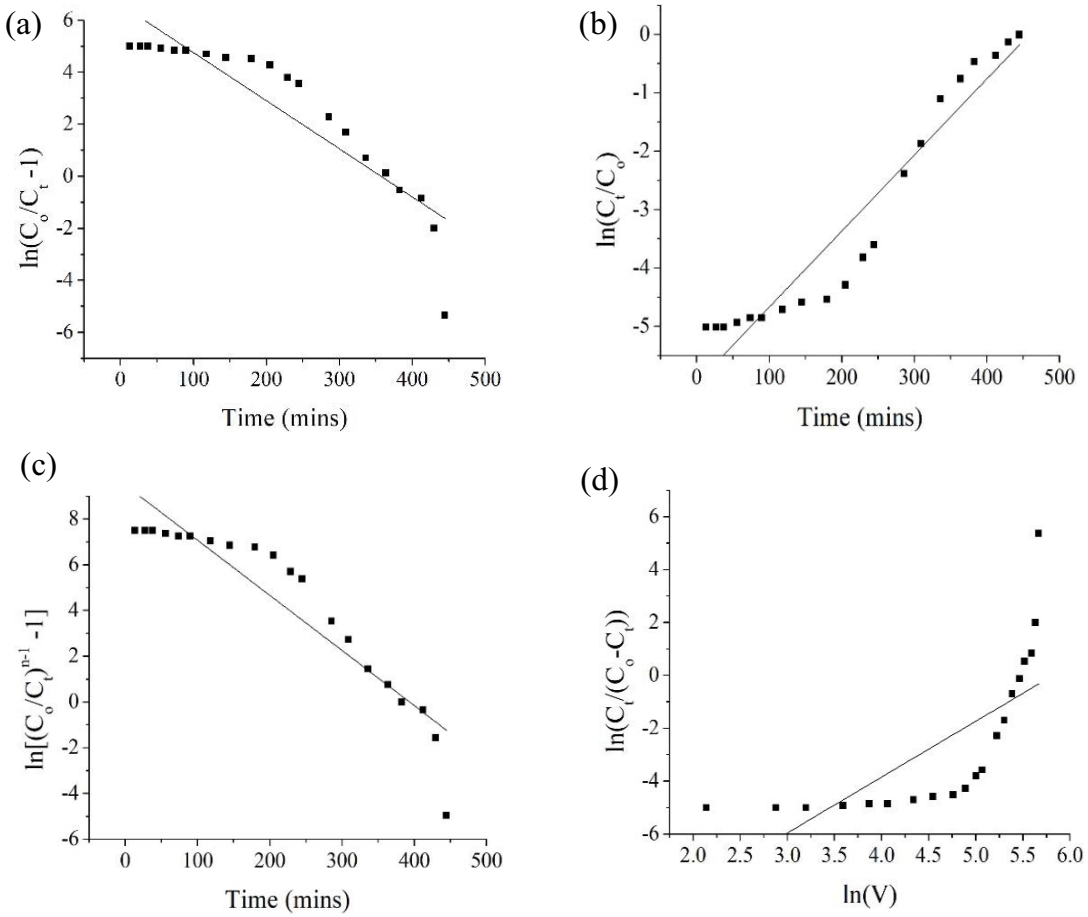

Fig. 16. (a) Thomas, (b) Bohart–Adams, (c) Clark, and (d) Yan model for fixed-bed adsorption of ASP using rGOM Flow rate = 0.65 mL min^{-1}; bed depth = 1.8 cm; pH = 3.0 ± 0.1; initial concentration = 100 mg L^{-1}; temperature = 25°C.

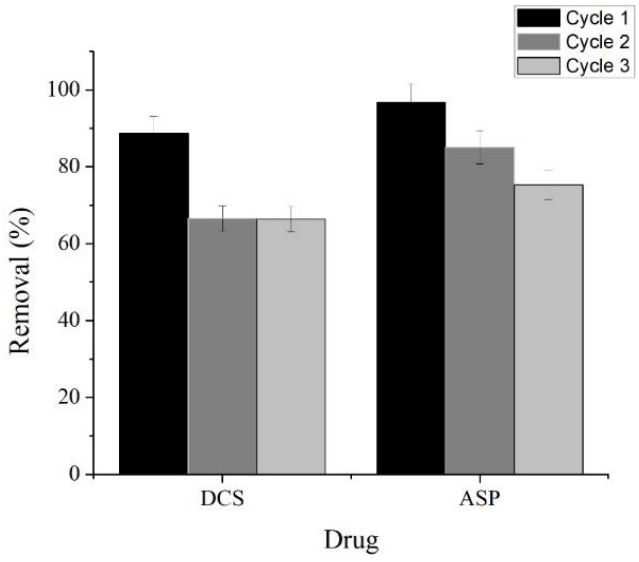

Fig. 17. Reusability study. Experimental conditions: shaker speed: 175 rpm; contact time = 40 min; pH = 5 ± 0.1 for DCS and 3 ± 0.1 for ASP; rGOM dosage = 14 g L^{-1} for DCS and 16 g L^{-1} for ASP; initial concentrations of DCS and ASP: 100 mg L^{-1}; temperature = 25°C.

high with almost 80% removal in the first 10 min. Batch adsorption experiments were conducted to find the optimum conditions for adsorption of both drugs. Different isotherm models were used to fit the adsorption data. Thermodynamic parameters of adsorption were calculated. Fixed-bed column adsorption was performed and fitted to well-known models. The study was concluded by investigating the optimum condition of rGOM regeneration. The results revealed that rGOM can be reused for more than three cycles without loss in its performance

References

[1] D.N. Lakdawalla, Economics of the pharmaceutical industry, J. Econ. Lit., 56 (2018) 397–449.
[2] P.E. Stackelberg, J. Gibs, E.T. Furlong, M.T. Meyer, S.D. Zaugg, R.L. Lippincott, Efficiency of conventional drinking-water-treatment processes in removal of pharmaceuticals and other organic compounds, Sci. Total Environ., 377 (2007) 255–272.
[3] B. Ferrari, N. Paxéus, R.L. Giudice, A. Pollio, J. Garric, Ecotoxicological impact of pharmaceuticals found in treated wastewaters: study of carbamazepine, clofibric acid, and diclofenac, Ecotoxicol. Environ. Saf., 55 (2003) 359–370.
[4] M. Iqbal, *Vicia faba* bioassay for environmental toxicity monitoring: a review, Chemosphere, 144 (2016) 785–802.
[5] M. Abbas, M. Adil, S. Ehtisham-ul-Haque, B. Munir, M. Yameen, A. Ghaffar, G. Abbas Shar, M. Asif Tahir, M. Iqbal, *Vibrio fischeri*

bioluminescence inhibition assay for ecotoxicity assessment: a review, Sci. Total Environ., 626 (2018) 1295–1309.
[6] M. Iqbal, M. Abbas, J. Nisar, A. Nazir, Bioassays based on higher plants as excellent dosimeters for ecotoxicity monitoring: a review, Chem. Int., 5 (2019) 1–80.
[7] M.J. Ahmed, Adsorption of non-steroidal anti-inflammatory drugs from aqueous solution using activated carbons: review, J. Environ. Manage., 190 (2017) 274–282.
[8] M. Bally, N. Dendukuri, B. Rich, L. Nadeau, A. Helin-Salmivaara, E. Garbe, J.M. Brophy, Risk of acute myocardial infarction with NSAIDs in real world use: bayesian meta-analysis of individual patient data, BMJ, 357 (2017) j1909, doi: 10.1136/bmj.j1909.
[9] L. Feng, E.D. van Hullebusch, M.A. Rodrigo, G. Esposito, M.A. Oturan, Removal of residual anti-inflammatory and analgesic pharmaceuticals from aqueous systems by electrochemical advanced oxidation processes. A review, Chem. Eng. J., 228 (2013) 944–964.
[10] M. Sarker, J.Y. Song, S.H. Jhung, Adsorptive removal of anti-inflammatory drugs from water using graphene oxide/metal-organic framework composites, Chem. Eng. J., 335 (2018) 74–81.
[11] A.M. Ali, L.K. Sydnes, W.M. Alarif, S.S. Al-Lihaibi, M.M. Aly, S.G. Aanrud, R. Kallenborn, Diclofenac and two of its photooxidation products in the marine environment: their toxicology and occurrence in Red Sea coastal waters, Environ. Chem. Ecotoxicol., 1 (2019) 19–25.
[12] K. Fent, A.A. Weston, D. Caminada, Ecotoxicology of human pharmaceuticals, Aquatic Toxicol., 76 (2006) 122–159.
[13] A.T. Banks, H.J. Zimmerman, K.G. Ishak, J.G. Harter, Diclofenac-associated hepatotoxicity: analysis of 180 cases reported to the food and drug administration as adverse reactions, Hepatology, 22 (1995) 820–827.
[14] J. Lindsay Oaks, M. Gilbert, M.Z. Virani, R.T. Watson, C.U. Meteyer, B.A. Rideout, H.L. Shivaprasad, S. Ahmed, M.J.I. Chaudhry, M. Arshad, S. Mahmood, A. Ali, A. Ahmed Khan, Diclofenac residues as the cause of vulture population decline in Pakistan, Nature, 427 (2004) 630–633.
[15] Y.Q. Leng, W.L. Guo, S.N. Su, C.L. Yi, L.T. Xing, Removal of antimony(III) from aqueous solution by graphene as an adsorbent, Chem. Eng. J., 211 (2012) 406–411.
[16] Y.J. Yoon, W.K. Park, T.-M. Hwang, D.H. Yoon, W.S. Yang, J.-W. Kang, Comparative evaluation of magnetite–graphene oxide and magnetite-reduced graphene oxide composite for As(III) and As(V) removal, J. Hazard. Mater., 304 (2016) 196–204.
[17] D.C. Marcano, D.V. Kosynkin, J.M. Berlin, A. Sinitskii, Z.Z. Sun, A. Slesarev, L.B. Alemany, W. Lu, J.M. Tour, Improved synthesis of graphene oxide, ACS Nano, 4 (2010) 4806–4814.
[18] K. Gupta, O.P. Khatri, Reduced graphene oxide as an effective adsorbent for removal of malachite green dye: plausible adsorption pathways, J. Colloid Interface Sci., 501 (2017) 11–21.
[19] R. Sitko, E. Turek, B. Zawisza, E. Malicka, E. Talik, J. Heimann, A. Gagor, B. Feist, R. Wrzalik, Adsorption of divalent metal ions from aqueous solutions using graphene oxide, Dalton Trans., 42 (2013) 5682–5689.
[20] G.Z. Kyzas, E.A. Deliyanni, D.N. Bikiaris, A.C. Mitropoulos, Graphene composites as dye adsorbents: review, Chem. Eng. Res. Des., 129 (2018) 75–88.
[21] J. Wang, B.L. Chen, Adsorption and coadsorption of organic pollutants and a heavy metal by graphene oxide and reduced graphene materials, Chem. Eng. J., 281 (2015) 379–388.
[22] A. Carmalin Sophia, E.C. Lima, N. Allaudeen, S. Rajan, Application of graphene based materials for adsorption of pharmaceutical traces from water and wastewater-a review, Desal. Water Treat., 57 (2016) 27573–27586.
[23] P.K. Boruah, D.J. Borah, J. Handique, P. Sharma, P. Sengupta, M.R. Das, Facile synthesis and characterization of Fe_3O_4 nanopowder and Fe_3O_4/reduced graphene oxide nanocomposite for methyl blue adsorption: a comparative study, J. Environ. Chem. Eng., 3 (2015) 1974–1985.
[24] L.A. Chacra, M.A. Sabri, T.H. Ibrahim, M.I. Khamis, N.M. Hamdan, S. Al-Asheh, M. AlRefai, C. Fernandez, Application of graphene nanoplatelets and graphene magnetite for the removal of emulsified oil from produced water, J. Environ. Chem. Eng., 6 (2018) 3018–3033.
[25] P.A. Webb, Introduction to Chemical Adsorption Analytical Techniques and their Applications to Catalysis, MIC Technical Publications, Micromeritics Instrument Corp., Norcross, Georgia 30093, 2003.
[26] A. Tayyebi, M. Outokesh, Supercritical synthesis of a magnetite-reduced graphene oxide hybrid with enhanced adsorption properties toward cobalt & strontium ions, RSC Adv., 6 (2016) 13898–13913.
[27] J.C. Moreno, R. Gómez, L. Giraldo, Removal of Mn, Fe, Ni and Cu ions from wastewater using cow bone charcoal, Materials, 3 (2010) 452–466.
[28] N. Ayawei, A.N. Ebelegi, D. Wankasi, Modelling and interpretation of adsorption isotherms, J. Chem., 2017 (2017) 1–11, https://doi.org/10.1155/2017/3039817.
[29] H.R. Wei, S.B. Deng, Q. Huang, Y. Nie, B. Wang, J. Huang, G. Yu, Regenerable granular carbon nanotubes/alumina hybrid adsorbents for diclofenac sodium and carbamazepine removal from aqueous solution, Water Res., 47 (2013) 4139–4147.
[30] Z. Hasan, N.A. Khan, S.H. Jhung, Adsorptive removal of diclofenac sodium from water with Zr-based metal–organic frameworks, Chem. Eng. J., 284 (2016) 1406–1413.
[31] C. Saucier, M.A. Adebayo, E.C. Lima, R. Cataluña, P.S. Thue, L.D.T. Prola, M.J. Puchana-Rosero, F.M. Machado, F.A. Pavan, G.L. Dotto, Microwave-assisted activated carbon from cocoa shell as adsorbent for removal of sodium diclofenac and nimesulide from aqueous effluents, J. Hazard. Mater., 289 (2015) 18–27.
[32] A. Khan, J. Wang, J. Li, X.X. Wang, Z.S. Chen, A. Alsaedi, T. Hayat, Y.T. Chen, X.K. Wang, The role of graphene oxide and graphene oxide-based nanomaterials in the removal of pharmaceuticals from aqueous media: a review, Environ. Sci. Pollut. Res., 24 (2017) 7938–7958.
[33] I.M. Jauris, C.F. Matos, C. Saucier, E.C. Lima, A.J.G. Zarbin, S.B. Fagan, F.M. Machado, I. Zanella, Adsorption of sodium diclofenac on graphene: a combined experimental and theoretical study, Phys. Chem. Chem. Phys., 18 (2016) 1526–1536.
[34] B.Y.Z. Hiew, L.Y. Lee, K.C. Lai, S.Y. Gan, S. Thangalazhy-Gopakumar, G.-T. Pan, T. Chung-KuangYang, Adsorptive decontamination of diclofenac by three-dimensional graphene-based adsorbent: response surface methodology, adsorption equilibrium, kinetic and thermodynamic studies, Environ. Res., 168 (2019) 241–253.
[35] K.-Y.A. Lin, H.T. Yang, W.-D. Lee, Enhanced removal of diclofenac from water using a zeolitic imidazole framework functionalized with cetyltrimethylammonium bromide (CTAB), RSC Adv., 5 (2015) 81330–81340.
[36] X. Hu, Z. Cheng, Removal of diclofenac from aqueous solution with multi-walled carbon nanotubes modified by nitric acid, Chin. J. Chem. Eng., 23 (2015) 1551–1556.
[37] S. Larous, A.-H. Meniai, Adsorption of Diclofenac from aqueous solution using activated carbon prepared from olive stones, Int. J. Hydrogen Energy, 41 (2016) 10380–10390.
[38] L.A. Al-Khateeb, S. Almotiry, M.A. Salam, Adsorption of pharmaceutical pollutants onto graphene nanoplatelets, Chem. Eng. J., 248 (2014) 191–199.
[39] T. Mukoko, M. Mupa, U. Guyo, F. Dziike, Preparation of rice hull activated carbon for the removal of selected pharmaceutical waste compounds in hospital effluent, J. Environ. Anal. Toxicol., S7 (2015) 008, doi: 10.4172/2161-0525.S7-008.
[40] S. Wong, Y.J. Lee, N. Ngadi, I.M. Inuwa, N.B. Mohamed, Synthesis of activated carbon from spent tea leaves for aspirin removal, Chin. J. Chem. Eng., 26 (2018) 1003–1011.
[41] K. Mphahlele, M.S. Onyango, S.D. Mhlanga, Adsorption of aspirin and paracetamol from aqueous solution using Fe/N-CNT/β-cyclodextrin nanocomopsites synthesized via a benign microwave assisted method, J. Environ. Chem. Eng., 3 (2015) 2619–2630.
[42] S.-H. Lee, O.H. Lin, R.-A. Doong, Design of size-tunable molecularly imprinted polymer for selective adsorption of acetaminophen, Clean Technol. Environ. Policy, 19 (2017) 243–250.
[43] A. Azman, N. Ngadi, D.K.A. Zaini, M. Jusoh, Z. Mohamad, A. Arsad, Effect of adsorption parameter on the removal of

aspirin using tyre waste adsorbent, Chem. Eng. Trans., 72 (2019) 157–162.
[44] R. Sips, On the structure of a catalyst surface, J. Chem. Phys., 16 (1948) 490–495, https://doi.org/10.1063/1.1746922.
[45] Y. Yu, Y.-Y. Zhuang, Z.-H. Wang, Adsorption of water-soluble dye onto functionalized resin, J. Colloid Interface Sci., 242 (2001) 288–293.
[46] T. Galaon, V. David, Deviation from van't Hoff dependence in RP-LC induced by tautomeric interconversion observed for four compounds, J. Sep. Sci., 34 (2011) 1423–1428.
[47] Ö. Kerkez-Kuyumcu, Ş.S. Bayazit, M.A. Salam, Antibiotic amoxicillin removal from aqueous solution using magnetically modified graphene nanoplatelets, J. Ind. Eng. Chem., 36 (2016) 198–205.
[48] S. Biswas, U. Mishra, Continuous fixed-bed column study and adsorption modeling: removal of lead ion from aqueous solution by charcoal originated from chemical carbonization of rubber wood sawdust, J. Chem., 2015 (2015) 1–9, https://doi.org/10.1155/2015/907379.
[49] H. Muhamad, H. Doan, A. Lohi, Batch and continuous fixed-bed column biosorption of Cd^{2+} and Cu^{2+}, Chem. Eng. J., 158 (2010) 369–377.
[50] M.A.E. de Franco, C.B. de Carvalho, M.M. Bonetto, R. de Pelegrini Soares, L.A. Féris, Diclofenac removal from water by adsorption using activated carbon in batch mode and fixed-bed column: isotherms, thermodynamic study and breakthrough curves modeling, J. Cleaner Prod., 181 (2018) 145–154.
[51] Z. Xu, J.-G. Cai, B.-C. Pan, Mathematically modeling fixed-bed adsorption in aqueous systems, J. Zhejiang Univ. Sci. A, 14 (2013) 155–176.